2.8 Å Crystal Structures of Recombinant Fibrinogen Fragment D with and without Two Peptide Ligands: GHRP Binding to the "b" Site Disrupts Its Nearby Calcium-binding Site†

Michael S. Kostelansky,‡ Laurie Betts,§ Oleg V. Gorkun,|| and Susan T. Lord*,‡,||

Department of Chemistry, Department of Pharmacology, and Department of Pathology and Laboratory Medicine, University of North Carolina, Chapel Hill, North Carolina 27599

Received May 24, 2002; Revised Manuscript Received July 9, 2002

ABSTRACT: We report two crystal structures, each at a resolution of 2.8 Å, of recombinant human fibrinogen fragment D (rfD) in the absence and presence of peptide ligands. The bound ligands, Gly-Pro-Arg-Pro-amide and Gly-His-Arg-Pro-amide, mimic the interactions of the thrombin exposed polymerization sites, "A" and "B", respectively. This report is the first to describe the structure of fragment D in the presence of both peptide ligands. The structures reveal that recombinant fibrinogen is nearly identical to the plasma protein but with minor changes, like the addition of a proximal fucose to the carbohydrate linked to residue βGln364, and slightly different relative positions of the β- and γ-modules. Of major interest in our structures is that a previously identified calcium site in plasma fibrinogen is absent when Gly-His-Arg-Pro-amide is bound. The peptide-dependent loss of this calcium site may have significant biological implications that are further discussed. These structures provide a foundation for the detailed structural analysis of variant recombinant fibrinogens that were used to identify critical functional residues within fragment D.

Fibrinogen, a 340 kDa soluble plasma protein, functions in vivo as the precursor to an insoluble fibrin clot. Fibrinogen is a dimeric protein, held together by 29 disulfide bonds. Each unit of the dimer consists of three nonidentical polypeptide chains, Aα, Bβ, and γ. The trinodular structure of the protein molecule (Figure 1A) can be described as two terminal D nodules each connected by a coiled coil to a central E nodule (*1*, *2*). The amino termini of the six chains originate in the central E nodule of the molecule, while the carboxyl termini of the Bβ- and γ-chains form independent modules in the D nodule (Figure 1A). The C-termini of the two Aα-chains (αC domains) have been shown to extend freely into solution or associate through noncovalent interactions with the central nodule (*3*). Crystal structures of modified bovine fibrinogen at 4 Å and native chicken fibrinogen at 2.7 Å (*2*, *4*) confirm early electron microscopy data that fibrinogen possesses a sigmoidal shape (*5*).

When the coagulation cascade is activated, fibrinogen is converted to fibrin by the serine protease, thrombin. Fibrin polymerization leads to development of an insoluble fibrin matrix, which, together with platelets, forms a hemostatic plug. The process of clot formation begins with thrombin cleavage of the amino termini of the Aα- and Bβ-chains releasing two pairs of peptides called fibrinopeptides A and B (FpA, FpB) (Figure 1A). The release of FpA exposes the N-terminal sequence of the α-chain (Gly-Pro-Arg-Val), called polymerization site "A", and the release of FpB exposes the N-terminal sequence of the β-chain (Gly-His-Arg-Pro), called polymerization site "B" (*6*). The "A" and "B" sites interact with the complementary binding sites, "a" and "b", located respectively in the γ- and β-modules in one D nodule of another molecule. The result of these "A:a" and "B:b" interactions is the formation of half staggered protofibrils aligning the D nodules of two molecules in one strand with the E nodule of a third molecule in a parallel strand (Figure 1B). Thereafter, the lateral aggregation of protofibrils forms a network of insoluble fibers. The existence of "A:a" and "B:b" interactions were corroborated in binding experiments with fibrinogen and short peptides (Gly-Pro-Arg-Pro and Gly-His-Arg-Pro), which mimic the "A" and "B" sites, respectively (*7*−*9*). Finally, clot structure is reinforced in vivo by cross-linking of γGln397 of one molecule to γLys406 of another molecule by Factor XIIIa (*10*).

Crystallographic study of fibrinogen has proven difficult. The challenges of crystallization have been primarily attributed to the flexibility of the αC domains. In recent years,

† This work was supported by National Institutes of Health Grant HL 31048 (S.T.L.). The atomic coordinates have been deposited in the Protein Data Bank (www.rcsb.org) under the access codes 1LT9 (rfD) and 1LTJ (rfD-BOTH).

* Corresponding author. Address: University of North Carolina at Chapel Hill, Department of Pathology and Laboratory Medicine, CB #7525, Brinkhous-Bullitt Building room 601, Chapel Hill, NC 27599-7525. Phone: (919) 966-3548. Fax: (919) 966-6718. E-mail: stl@med.unc.edu.

‡ Department of Chemistry.

§ Department of Pharmacology.

|| Department of Pathology and Laboratory Medicine.

[1] Abbreviations: rfD, recombinant fibrinogen fragment D; rfD-BOTH, recombinant fibrinogen fragment D with GPRPam and GHRPam bound; GPRPam, Gly-Pro-Arg-Pro-amide; GHRPam, Gly-His-Arg-Pro-amide; FpA, fibrinopeptide A; FpB, fibrinpeptide B; HEPES, N−(hydroxyethyl)piperazine-N′(2-ethanesulfonic acid); GPRPAA, Gly-Pro-Arg-Pro-Ala-Ala; GlcNAc, *N*-acetylgalactosamine; Man, Mannose; EDTA, ethylenediaminetetraacetic acid.

10.1021/bi0261894 CCC: $22.00
Published on Web 09/10/2002

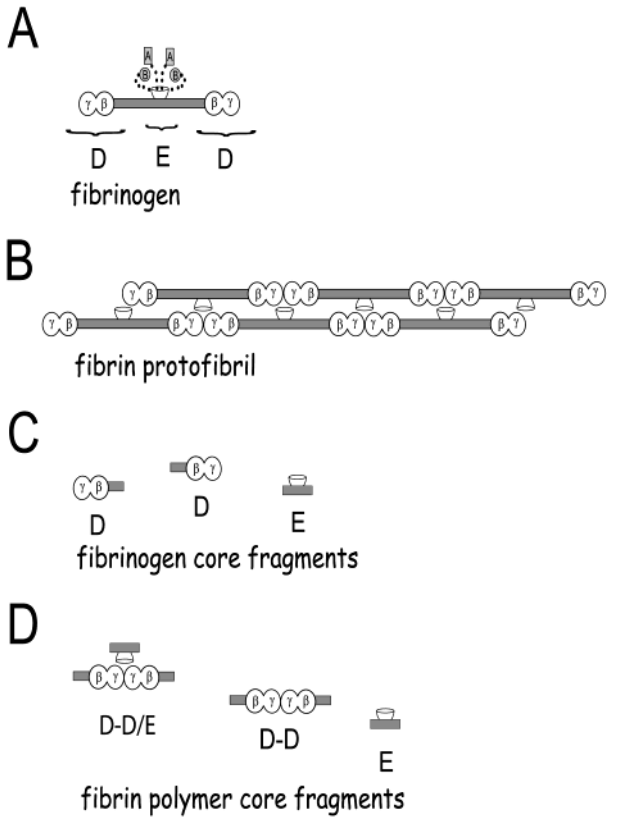

FIGURE 1: Depiction of fibrinogen, a fibrin protofibril, and core degradation fragments of fibrinogen/fibrin. Panel A shows the fibrinogen molecule. The central nodule (E) contains fibrinopeptide A (A, gray box) and fibrinopeptide B (B, gray circle). Distal nodules (D) are composed of the C-terminal regions of the gamma chain (γ) and beta chain (β). Gray box represents the coiled coil region connecting the E and D nodules. Panel B shows a protofibril composed of double stranded half-staggered fibrin molecules. Panel C depicts core degradation fragments of fibrinogen generated by proteolytic enzymes. Fragment D (D) contains the β- and γ-modules and a portion of the coiled coil region and represents the distal part of the fibrinogen molecule. Fragment E (E) is composed of the N-termini of all polypeptide chains and a portion of the coiled coil region and represents the central nodule of the molecule. Panel D shows core proteolytic fragments generated by the degradation of fibrin. The D−D/E fragment consists of Factor XIIIa cross-linked D fragments bound noncovalently to fragment E. The D−D/E complex can be dissociated to D−D and fragment E.

one strategy to overcome this challenge was to eliminate αC domains by proteolysis of human plasma fibrinogen and fibrin polymer. Core degradation fragments (Figure 1C,D) of the D and E regions of the molecule can be generated with various proteases (*1*, *11*, *12*). These core fragments retain large portions of native structure that exist in fibrinogen making them suitable for crystallographic study. These fragments were crystallized alone or in the presence of peptides derived from the N-terminal sequences of fibrin's α- and β-chains. Previously determined human fibrinogen fragment crystal structures include a recombinant 30 kDa portion of the γ-module (*13*, *14*), an 86 kDa proteolytically generated fragment D (Figure 1C), which includes the D nodule and a portion of the coiled coil (*15*−*17*), and a 170 kDa cross-linked double-D fragment from fibrin (Figure 1D) (*15*−*17*). These studies confirm and give structural evidence for two interactions that occur at the D−D/E interface of a protofibril (Figure 1B,D): (1) the interaction of the "A" site (Gly-Pro-Arg) bound to the γ-module (*14*, *15*) and (2) the staggered end-to-end interaction that occurs between two cross-linked γ-modules (*15*). The interaction of the "B" site (Gly-His-Arg) bound in a pocket located in the β-module was also revealed (*16*, *17*); however, the importance of this interaction in polymerization is not fully understood. Additionally, these studies showed that the Aα-chain reverses direction at the C-terminal disulfide ring to form a fourth α-helical strand that reaches back toward the center of the molecule and is an integral part of the coiled-coil connector (*15*). This is consistent with the location of αC domains near the center of the molecule (*18*−*20*).

Protein engineering has been used to identify residues and domains critical to fibrinogen's many functions. For example, engineered variant fibrinogens have been developed to examine residues thought to be important for thrombin binding to fibrinogen, fibrinogen-mediated platelet aggregation, and "A:a" interactions (*21*−*25*). Variant fibrinogens based on naturally occurring and novel mutations have aided in dissecting fibrinogen function. The conclusions of these studies rely on the assumption that recombinant fibrinogen is structurally identical to plasma fibrinogen. This assumption is quite reasonable; however, the possibility exists that it may not be accurate. For example, posttranslational modification of the recombinant protein during synthesis may lead to functionally significant differences compared to plasma protein (*26*). In biochemical studies, Gorkun et al showed that recombinant fibrinogen served as an accurate model for plasma fibrinogen (*27*). However, to date there have been no direct structural data to assess whether recombinant fibrinogen is identical to plasma fibrinogen.

We have now determined 2.8 Å X-ray crystal structures of both recombinant human fibrinogen fragment D (rfD) and recombinant human fibrinogen fragment D cocrystallized with both GPRPam and GHRPam (rfD-BOTH). Notably, we present the first structure of fragment D in the presence of both GPRPam and GHRPam. The structures reveal that recombinant fibrinogen fragment D is similar to the plasma fibrinogen structures previously determined, but with significant differences in a calcium-binding site which will be described.

MATERIALS AND METHODS

All chemicals were of reagent grade and, unless specified, were purchased from Sigma (St. Louis, MO). GPRPam and GHRPam peptides were purchased from the Protein Chemistry Laboratory of University of North Carolina (Chapel Hill, NC). Recombinant fibrinogen media was obtained from the National Cell Culture Center (Minneapolis, MN).

Expression and Purification of Recombinant Fibrinogen. Recombinant fibrinogen was synthesized as described previously (*22*), in Chinese hamster ovary cells harboring cDNA for the Aα-, Bβ-, and γ-chains of human fibrinogen. Large-scale expression was carried out in serum-free medium in roller bottles. Media containing secreted protein were harvested, and protease inhibitors were added (*21*). The medium was then frozen and stored at −20 °C.

Recombinant fibrinogen was purified from the medium by ammonium sulfate precipitation followed by immunoaffinity chromatography using IF-1 monoclonal antibody (Iatron Corp., Tokyo, Japan) linked to Sepharose 4B (Amersham-Pharmacia-Biotech, Piscataway, NJ). Fibrinogen was

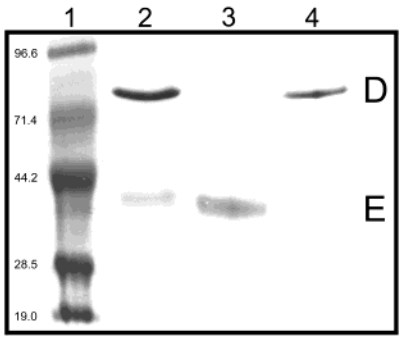

FIGURE 2: SDS−PAGE of rfD purification. Samples were run on a gradient 4−15% Pharmacia Phast Gel. Molecular mass markers (kDa), lane 1. Trypsin digest of recombinant fibrinogen used to obtain rfD, lane 2. Purified fragment E (E), lane 3. Purified rfD (D), lane 4.

eluted from the column with buffer containing 5 mM EDTA (*27*, *28*). The isolated protein was extensively dialyzed against HEPES buffer (20 mM HEPES, pH 7.4, 150 mM NaCl), aliquoted, and stored at −70 °C. To confirm purity and proper polypeptide chain composition of the recombinant protein, SDS−PAGE analysis under reduced and nonreduced conditions was performed as described by Laemmli (*29*).

Preparation and Purification of Recombinant Fibrinogen Fragment D. $CaCl_2$ (final concentration of 20 mM) was added to 11 mg of recombinant fibrinogen (final concentration of 0.44 mg/mL) in HEPES buffer. rfD preparation was initiated by adding 125 μL of immobilized TPCK Trypsin (Pierce, Rockford, IL). The reaction proceeded over a period of days and was monitored by SDS−PAGE analysis. The reaction was stopped by removing the beads with immobilized trypsin when only rfD and E fragments were seen on the SDS−PAGE (Figure 2). The beads were removed from the digest by filtering through a 0.22 μm syringe fitting filter (Costar, Corning, NY). The digest was then frozen at −70 °C.

Recombinant fragment D was purified by peptide affinity chromatography based on a method described by Everse et al (*30*). A polymeric resin with the peptide GPRPAA covalently linked to it served as the affinity matrix (personal communication Dr. David Klapper, UNC, Chapel Hill, NC). Approximately 2 mL of resin prepared by the UNC−CH Microprotein Facility was placed in a polypropylene column (diameter of 1.6 cm). Eleven milligrams of trypsin digested fibrinogen was loaded on the column equilibrated with HEPES buffer containing 20 mM $CaCl_2$ at a flow rate of 10 mL/hr. The column was washed with 10 volumes of the loading buffer, and rfD was eluted with 1 M NaBr, 50 mM sodium acetate, pH 5.3. Fractions containing rfD were pooled and dialyzed against 50 mM Tris, pH 7.0 (Figure 2). The protein was then concentrated with a centrifugal filter device (10 kDa MW cutoff, Millipore Corp., Bedford, MA) and was stored at 4 °C. Amino terminal sequencing of rfD was performed by Dr. Dave Klapper (UNC, Chapel Hill, NC).

Crystallization of Recombinant Fragment D. Crystals of rfD were grown by sitting-drop vapor diffusion at 4 °C. Crystallization conditions were derived by screening conditions based on those reported for plasma fibrinogen-generated fragment D crystals (*15*, *30*) and those reported for the recombinant γ-module (*13*). The concentration of fragment D was 12 mg/mL, while the wells contained 50 mM Tris, pH 8.5, 2 mM NaN_3, 70 mM $CaCl_2$, and 8−15% PEG 3350 (wt/vol); drops contained 5 μL of protein and 5 μL of well solution. Crystals were obtained at 8−15% PEG concentrations, but large single crystals grew best at 9% PEG. Streak seeding was employed to maximize crystal size and quality. Diffraction quality crystals, with approximate dimensions of 0.25 mm × 0.25 mm × 0.025 mm, appeared in about 1 week.

Crystals of recombinant fragment D in the presence of two synthetic peptides (rfD-BOTH), GHRPam and GPRPam, were also grown at 4 °C. Sitting drops were prepared by mixing 5 μL of protein solution, containing fragment D at 12 mg/mL (0.15 mM) in 50 mM Tris, pH 7.0, 2 mM GHRPam, and 2 mM GPRPam, with 5 μL of well solution containing 50 mM Tris, pH 8.5, 2 mM NaN_3, 12.5 mM $CaCl_2$, and 7% PEG 3350. Large single crystals appeared in a week. Seeding again increased the yield of quality crystals.

Data Collection at 100°K. Diffraction data for both rfD and rfD-BOTH were collected at 100°K using a Rigaku RUH3R rotating anode generator with Osmic confocal blue multilayer optics and Rigaku R-AXIS IV^{++} detector. The crystals were prepared for low-temperature data collection by cryoprotecting in a solution that contained the crystallant plus 20% gylcerol. The crystals were then flash frozen in liquid nitrogen. Resulting data sets were processed using DENZO and SCALEPACK (*31*).

Structure Determination. The structure of rfD-BOTH was determined by molecular replacement using AMoRe (*32*). One molecule from the cross-linked plasma double-D fragment with ligands bound (PDB code = 1FZC) was used as a search model. To account for the shorter chain length of our recombinant fragment D, the search model was altered by deleting residues α119−125. A rotation search using data from 8 to 4.0 Å was performed, yielding one clear solution for the rotation function at 12.8 σ above the mean and two strong solutions to the translation function at 11.0 and 23.6 σ, respectively. The correlation coefficient and *R*-factor after rigid-body fitting were 52.4 and 45.6, respectively. Similar unit cell dimensions exist for both the rfD and rfD-BOTH crystals, therefore allowing the rfD structure to be solved by rigid-body refinement using the refined structure of rfD-BOTH. The asymmetric unit of both $P2_12_12_1$ crystals consists of two fragment D molecules. They are oriented in almost the same direction, hence the single peak in the cross-rotation function, but their translations are staggered along the *a* and *c* axes.

The structures were refined using CNS, including an overall anisotropic *B*-factor and a bulk solvent correction (*33*). Additionally, for the first round of refinement, noncrystallographic symmetry restraints were used. For both structures, 5% of the observed data was set aside for cross-validation using the free *R*-factor statistic before any refinement (*34*). After the first round of refinement in CNS, manual fitting of rfD and rfD-BOTH was performed using the program O (*35*) and sigmaA-weighted $|2F_o-F_c|$ and $|F_o-F_c|$ electron density maps (*36*). The working *R*-factor and free *R*-factor were monitored to guide the progress of rebuilding as each cycle of manual rebuilding followed by refinement was carried out. Finally, in the last stages of refinement, 146 and 250 solvent sites were added to the structures of rfD and rfD-BOTH, respectively.

Table 1: Crystallographic Data and Refinement Statistics

	rfD	rfD-BOTH
resolution (Å)	18−2.8	18−2.8
space group	$P2_12_12_1$	$P2_12_12_1$
cell constants (Å)	$a = 88.7$	$a = 89.3$
	$b = 94.5$	$b = 94.2$
	$c = 227.1$	$c = 226.9$
molecules /asymmetric unit	2	2
total observations	217,604	181,953
unique reflections	47,742	46,717
mean redundancy	4.6	3.9
R_{sym}[a] (%; highest shell)	11.0 (54.0)	12.3 (39.3)
completeness (%; highest shell)	99.9 (99.9)	97.8 (92.8)
mean I/σ (highest shell)	14.0 (3.1)	13.8 (2.9)
R_{cryst}[b] (%)	22.4	21.2
R_{free}[c] (%)	27.1	27.0
RMSD bond lengths (Å)	0.0068	0.0066
RMSD bond angles (^{o})	1.27	1.28
average B-factor	47.2	45.0
number of model atoms	10,623	10,899
number solvent sites	146	250

[a] $R_{sym} = \Sigma|I - \langle I\rangle|$, where I is the observed intensity and $\langle I\rangle$ is the average intensity of multiple symmetry-related observations of that reflection. [b] $R_{cryst} = \Sigma||F_{obs}| - |F_{calc}||/\Sigma|F_{obs}|$, where F_{obs} and F_{calc} are the observed and calculated structure factors, respectively. [c] $R_{free} = \Sigma||F_{obs}| - |F_{calc}||/\Sigma|F_{obs}|$ for 5% of the data withheld from structural refinement.

RESULTS

Recombinant Fragment D. We determined that rfD is shorter in the coiled-coil region of the molecule compared to plasma-generated fragment D. The sequence of plasma-generated fragment D was reported to be α111−197, β134−461 and γ88−406 (*15*). We determined the amino terminal residues of rfD to be a mixture of αLys125 and αVal126, βHis149, and γTyr96 (data not shown). The C-termini of rfD chains were not sequenced. Previously reported data for plasma fragment D (*15*), together with the possible trypsin cleavage sites and visible electron density, suggested the C-termini of rfD were αLys191, βGln461, and γLys406. The sequence-derived molecular weight for rfD is 79 kDa, which is in good agreement with the molecular weight determined from SDS−PAGE (data not shown). The electron density maps allowed us to model residues α126−190, β161−458, and γ96−394.

General Structural Features. We crystallized rfD in the absence and presence of two peptide ligands which model the "A" and "B" polymerization sites. The rfD-BOTH structure was solved by molecular replacement using one molecule of the structure of the cross-linked double-D fragment with ligands bound (1FZC) as described in the methods. The structure of rfD was solved by rigid-body refinement using the refined rfD-BOTH structure as a starting model, followed by simulated annealing refinement. The space group for rfD and rfD-BOTH is $P2_12_12_1$ (Table 1). The unit cell dimensions for the rfD crystal were $a = 88.7$ Å, $b = 94.5$ Å, and $c = 227.1$ Å, while those for rfD-BOTH differed by less than an angstrom in each dimension. These unit cell dimensions are different from those previously reported for plasma fibrinogen-generated fragment D crystals (*17*). The new crystal form has different packing, likely due to the shortened chains in the coiled-coil region of rfD.

rfD is similar in structure to the plasma-generated fragment (Figures 3 and 4) (*15*). The N-termini of the three chains

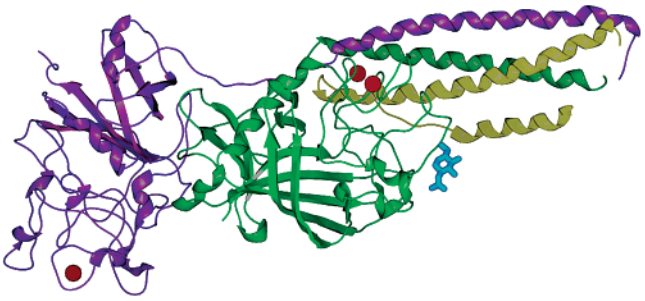

FIGURE 3: Ribbon diagram of rfD molecule. The α-chain is yellow, the β-chain is green, and the γ-chain is purple. Calcium atoms are depicted as red circles, while the carbohydrate moiety is drawn in blue.

forms a coiled coil, which is augmented by a fourth α-helical segment of the α-chain that doubles back at residue αSer166. The C-terminal portions of the β- and γ-chains fold into two independent globular modules. The γ-module extends outward away from the coiled coil, while the β-module remains close to the coiled coil. The β- and γ-modules each contain a cis peptide bond at residues βCys407 and γCys339, respectively. In contrast to plasma-generated fragment D structures, the α-helical structure of the N-terminus of γ-chain residues γTyr96 to γLeu101 is disrupted. This part of the chain is unwound, and at residue γLeu101, an ∼90° bend is made. This bend allows for packing interactions between the two molecules in the asymmetric unit.

Our rfD structure was compared to the structure of plasma fibrinogen fragment D (1FZA). The root-mean-square deviation (RMSD) between one molecule of each structure was 1.7 Å over all atoms. When examining the aligned structures, the most obvious differences between the molecules were in loop regions. We attribute these differences to a disparity in the accuracy of the two models. R_{cryst} and R_{free} for the 2.9 Å plasma fragment D structure are 26.3% and 36.3%, respectively (*15*). This 10% deviation between R_{cryst} and R_{free} suggests that this early model of the molecule contained errors that were corrected in later plasma fragment D structures. The better-quality R_{cryst} (22.4%) and R_{free} (27.1%) statistics for the 2.8 Å rfD structure suggest that our model is more accurate than the plasma fragment D structure.

Our rfD-BOTH structure was compared to the plasma fibrinogen cross-linked double-D structure with ligands bound (1FZC). We found the structure of rfD-BOTH to be isomorphous with the plasma fibrinogen double-D structure. When one molecule of rfD-BOTH is aligned with one molecule from the plasma fibrinogen double-D structure, the all-atom RMSD is 1.2 Å. When the Cα atoms of only the β-modules are aligned, the RMSD for these modules is significantly improved to 0.48 Å. Visual inspection (Figure 4) of the β-module alignment reveals that the orientation of the β- and γ-modules in rfD-BOTH differs by a few degrees from the orientation of these modules in the plasma double-D structure. This difference can be attributed to alternate packing interactions due to our new crystal form.

Peptide Ligands. The rfD-BOTH structure is novel because it is the first reported non-cross-linked fragment D structure cocrystallized with both peptide ligands mimicking the "A" and "B" polymerization sites. The presence of GPRPam in the "a" site and GHRPam in the "b" site are clear in the $|F_o - F_c|$ maps (Figure 5A,B). Several conformational changes

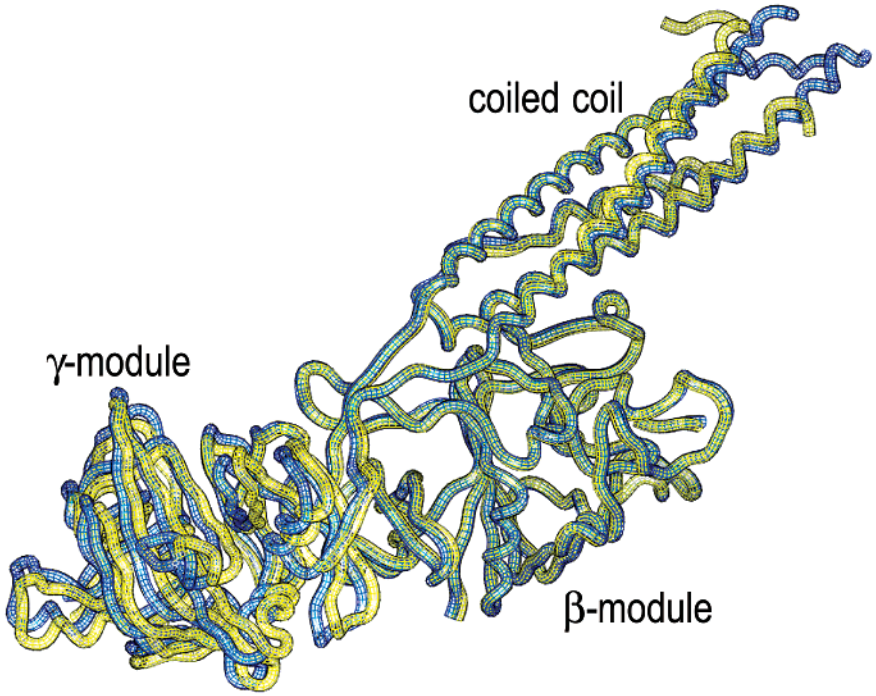

FIGURE 4: Worm diagrams of rfD-BOTH (yellow) and plasma double-D with ligand bound (1FZC, blue), aligned by the β-module Cα-atoms. The RMSD for the β-module alignment is 0.48 Å, and the corresponding γ-modules of the two structures showed a shift in their positions. The β-, γ-module and the coiled-coil region are labeled.

reported for plasma fibrinogen (*16*, *17*), (1) a shift in residue γTyr363 upon binding GPRPam and (2) the 180° flip of βGlu397 and βAsp398 toward GHRPam, occur similarly in recombinant fibrinogen fragment D.

Calcium Sites. The rfD crystal structure confirmed the presence of three calcium-binding sites as previously identified in plasma fibrinogen studies, with one in the γ-module and two in the β-module (*17*). All three sites are fully occupied with calcium in the unliganded structure. The γ-module site is located adjacent to the "a" site and includes residues γAsp318 and γAsp320 and backbone carbonyls of γPhe322 and γGly324. One β-module calcium site is at a position homologous to the γ-module calcium site and includes the side chains of residues βAsp381 and βAsp383 and the backbone carbonyl oxygen of βTrp385. Our data show that the second calcium site in the β-module, adjacent to the "b" site, is comprised of the side chains of residues βAsp398, βAsp261, and γGlu132 and the backbone carbonyl oxygen of βGly263. This model differs from the previous study, which stated that βGlu397 was a coordinating residue at this site rather than βGly263 (*17*). Nevertheless, a comparison of the calcium-binding site adjacent to the "b" site in the structure 1FZE (a double-D fragment with no ligands bound) with this site in our rfD model showed these structures are in agreement. Both models reveal that βGlu397 is 6−7 Å away from the calcium atom, while the βGly263-calcium distance is only ~2.4 Å. These observations clearly suggest the fourth calcium coordinate at this site is βGly263 and not βGlu397. The basis for the previous identification of βGlu397 as a coordinator of calcium is unclear.

In the rfD-BOTH structure, only two calcium ions per D fragment are present. When GHRPam binds to the "b" site, residue βAsp398 is pulled away from its coordination position in the calcium-binding site. Concomitantly, γGlu132 moves approximately 1 Å away from its coordination position and forms a salt-link with αLys157 (Figure 6). The loss of these two calcium ligands and lack of strong $|F_o - F_c|$ density at this site suggests that in the presence of peptide, calcium is no longer bound at this site, and instead a water molecule now bridges residues βAsp261 and βGly263, as shown in Figure 6. To assess this interpretation, we modeled the site with and without calcium. With calcium bound at this site in both molecules of the asymmetric unit, the temperature factors for these calcium atoms are 85 and 106 Å^2, respectively. These high-temperature factor values suggest that either calcium is incorrectly modeled at this site or the site has a low occupancy. Although partial occupancy in the crystal remains a possibility, our data indicate that under physiologic conditions calcium is not bound at this site when the "b" site is occupied because the concentration of calcium in the crystallant (12.5 mM) is 5 times that of plasma levels. Thus, our modeling showed a better fit of the data when this calcium is eliminated upon binding GHRPam and in its place a water molecule bridges residues βAsp261 and βGly263.

Carbohydrate. A clear difference between plasma fibrinogen and recombinant fibrinogen is revealed by the structure of rfD-BOTH. Upon binding of the peptide GHRPam, the electron density of the carbohydrate linked to βGln364 improves, probably due to reduced movement of the carbohydrate because of its proximity to His in GHRPam. The improved electron density reveals the presence of additional density which we have interpreted as an α(1,6) fucose linkage to the first GlcNAc in the chain (Figure 7). Previous biochemical studies on plasma fibrinogen characterized the carbohydrate linked in this position to be of the biantennary type where the first three sugars are GlcNAc, GlcNAc, and Man (*37*). Therefore, the rfD-BOTH data suggest that recombinant fibrinogen possesses an altered carbohydrate cluster on βGln364.

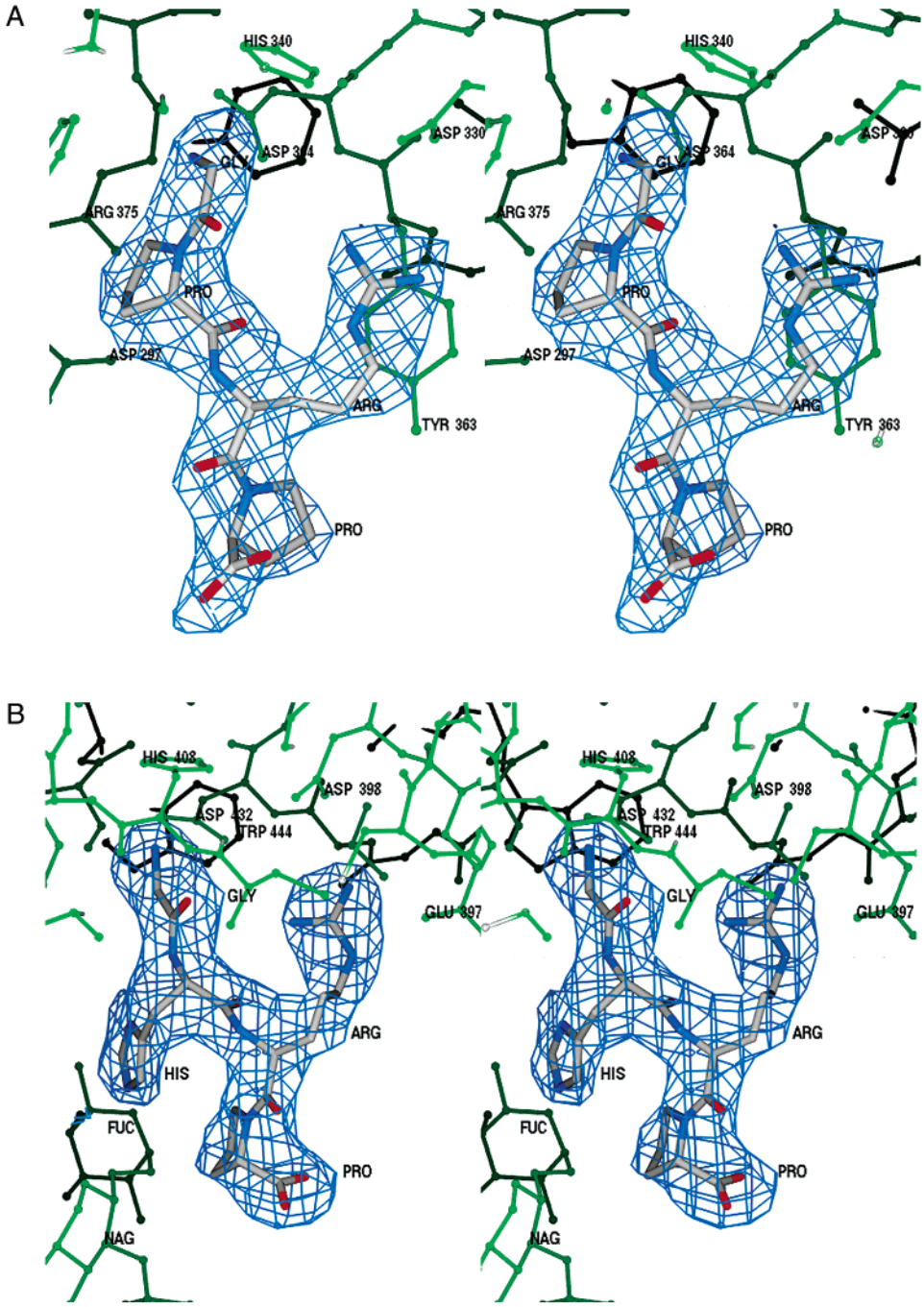

FIGURE 5: Electron density for the peptide ligands from the rfD-BOTH structure. Stereodiagrams of $|F_o-F_c|$ electron density showing (A) GPRP present in the γ-chain binding site and (B) GHRP present in the β-chain binding site. Maps are contoured at 2.5 σ.

DISCUSSION

The structure determination of recombinant fibrinogen fragment D was undertaken to determine whether our engineered protein is identical in structure to the plasma protein and to provide a basis for interpretation of past and future studies of variant recombinant fibrinogens. We were able to crystallize fragment D in the presence of ligands and report here, for the first time, a structure of a single fragment D with both GPRPam and GHRPam bound. This structure is isomorphous with the structure of the covalently linked, plasma-generated double-D fragment with two ligands bound. Interestingly, the structural similarity between rfD-BOTH and plasma-generated double-D with ligands bound implies that neither cross-linking nor the established D−D interface dramatically changes this region of the molecule. The structural data for rfD and rfD-BOTH revealed that the recombinant protein is nearly identical to the plasma protein, with a small number of exceptions. Notably, our recombinant protein data reveal the addition of an α(1,6) fucose linkage to the N-linked carbohydrate on residue βGln364. The addition of this proximal α(1,6) fucose has been observed to occur in other recombinant proteins synthesized in Chinese hampster ovary cells (*38*, *39*).

The structural data for rfD-BOTH suggest different conformational changes at the "b" site from those previously reported for plasma-generated fragment D with GHRPam bound (*17*). Specifically, the calcium site in rfD-BOTH adjacent to the "b" site is lost upon binding of GHRPam,

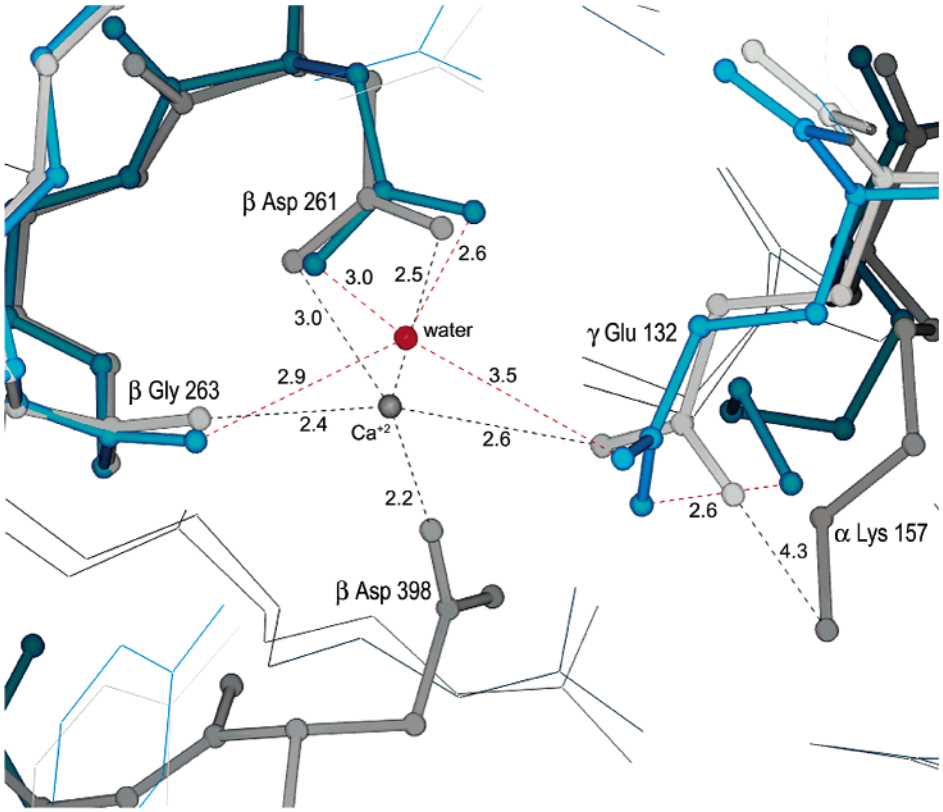

FIGURE 6: Superimposed structures of rfD and rfD-BOTH showing the calcium-binding site adjacent to the "b" site in the absence and presence of GHRPam. Residues colored in gray are positions of residues in the absence of GHRPam, while those depicted in blue are positions of the residues in the presence of GHRPam. The calcium atom is gray, while the water molecule replacing calcium in the presence of GHRPam is depicted as a red atom. Distances between residues and calcium (black dashes) and between residues and water (red dashes) are in angstroms. Note the loss of calcium in the presence of GHRPam resulting from the loss of coordinator βAsp398 upon GHRPam binding and the formation of a new salt-link between γGlu132 and αLys157.

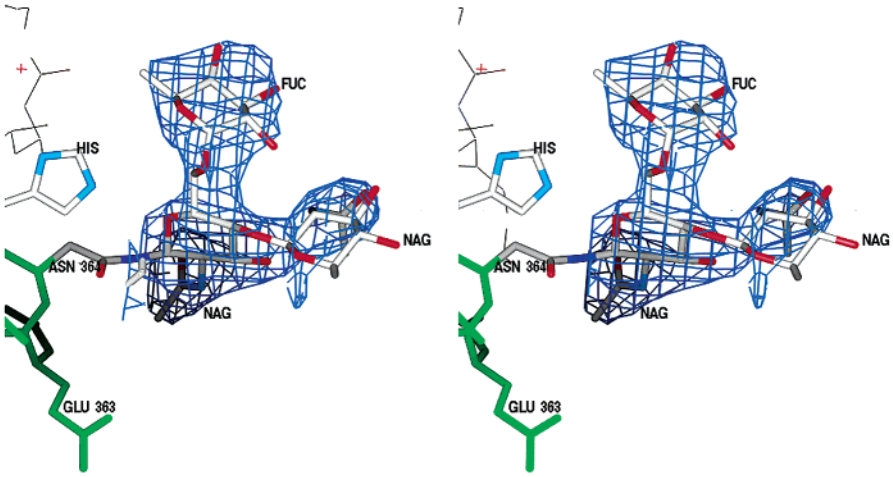

FIGURE 7: Electron density for the carbohydrate linked to βGln364 in the rfD-BOTH structure. The $|F_o - F_c|$ electron density map is contoured at 2.0 σ. A proximal α(1,6) fucose (FUC) is shown linked to the first *N*-acetylgalactosamine (NAG). Histidine residue (HIS) is from GHRPam bound in the "b" site.

with changes in the positions of two coordinating residues, βAsp398 and γGlu132. βAsp398 flips to interact with the GHRPam upon binding, as previously reported, and γGlu132 moves to form a new salt-link with residue αLys157. A water molecule now bridges the two remaining coordinating residues, βAsp261 and βGly263. Our interpretation of the structural data differs from a prior report which states that calcium remains bound at this site in the presence of GHRPam (*17*). Unfortunately, structure factors for the plasma fibrinogen structures are not in the Protein Data Bank, so we cannot directly compare electron density data for plasma fragment D to our own data. Instead, we compared the temperature factors of the reported plasma structures and our structure with calcium modeled at this site. We found that the temperature factors are similar, suggesting to us that our data is analogous to previous data. The high-temperature factors ranging from 71 to 106 Å^2 for these sites modeled with calcium suggest very low occupancy of the site or that calcium would be modeled incorrectly at this site. Considering the weak density and loss of two coordinating residues,

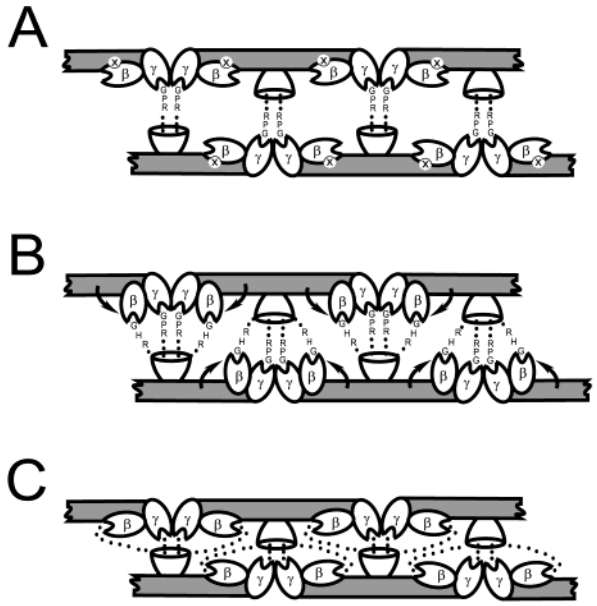

FIGURE 8: Models of interactions occurring at the D−D/E interface of a fibrin protofibril. (A) A diagram of a fibrin protofibril held together by "A:a" interactions (GPR···). Without the "B:b" interaction, the β-module (β) is anchored to the coiled coil (gray box) by the calcium site adjacent to the "b" site (circle with x). (B) A fibrin protofibril held together by both "A:a" (GPR···) and "B:b" (GHR···) interactions. With the "B:b" interaction, the calcium site is now abolished, and the β-module (β) can move away from the coiled coil connector (gray box) upon interactions related to the D−D/E interface (arrows). (C) A fibrin protofibril based on two current models of fibrinogen polymerization (*40*, *44*) that includes both "A:a" and "B:b" interactions (···), but the position of the β-module (β) is unchanged from that of fibrinogen.

we suggest there is no calcium bound at this site in the presence of GHRPam.

The loss of the calcium-binding site when GHRPam binds to the "b" site implies that functionally significant consequences are associated with this event. This calcium site is positioned where all three polypeptide chains are in close contact. The calcium atom appears to anchor the β-module by residues βAsp398, βAsp261, and βGly263 to the γ-chain coiled coil through residue γGlu132.

On the basis of the novel observation that calcium is lost upon binding GHRPam, we propose that this calcium atom serves as an "anchor", which tethers the β-module to the coiled coil in a specific "monomer" conformation in this part of the molecule, as shown in Figure 8A. During polymerization, the N-terminus of the β-chain binds to the "b" polymerization site ("B:b" interaction) with the subsequent loss of calcium. In the absence of this anchor, the β-module has new freedom of motion in relation to the other parts of the molecule, such that the β-module can assume a "polymer" conformation. As shown in Figure 8B, the β-modules on two adjacent fibrin molecules can then interact with the E nodule of another fibrin molecule. These two "B:b" interactions thus link the same three fibrin monomers as the earlier "A:a" interactions. Further, the change in conformation of the β-module will expose novel sites that may be critical for lateral aggregation, as recently proposed by Yang et al (*40*).

We propose that the loss of this calcium anchor is one important step in a series of events in the conversion of a fibrin monomer into a polymer, as "B:b" interactions are not required for fibrin polymerization. For example, the conversion of fibrinogen to fibrin can be catalyzed by reptilase, which removes only FpA. Nevertheless, the morphology of reptilase clots differs from that of thrombin clots (*41*), and we propose that this difference reflects the disruption of the calcium anchor upon "B:b" binding in combination with a conformational change in the β-module.

The proposed change in orientation of the β-module is consistent with early publications that reported conformational changes in the D nodule associated with the conversion of monomer to polymer. For example, Donovan and Mihalayi in calorimetric studies concluded that polymerization is accompanied by conformational changes in the D nodule of a fibrin clot (*42*). We propose that the loss of the calcium anchor is a part of these conformational changes, and without this calcium the fibrin molecule has a more flexible conformation. More recent biochemical studies reveal the exposure of residues in the coiled coil region which are also linked to movement of the β-module upon forming a polymer. Yakovlev et al. have shown that the coiled coil region α148−160 is exposed in the D−D/E complex but not in fragments D and cross-linked D−D (*43*). They suggest that during polymerization the β-module moves away from coiled coil connector in the fibrin molecule to make α148−160 accessible. When considered with our data, the movement of the β-module in the D−D/E complex relative to fragment D or D−D is tied to the loss of the calcium anchor. Thus, these previous reports are consistent with our proposed model in Figure 8 panel B, rather than that in panel C where the position of the β-module in relation to the coiled coil is not different from fibrinogen. The model in Figure 8C is based on a combination of two models, (1) proposed from analysis of plasma fibrinogen D−D crystal structures (*40*) and (2) a model proposed by Madrazo et al from the analysis of a bovine E nodule structure (*44*).

Another motivation for this study lies in our use of variant fibrinogens to identify the roles of certain residues in fibrinogen function (*28*, *45*−*47*). To date, we have made and characterized many variant fibrinogens with mutations in the D nodule. When carrying out mutagenesis experiments, the possibility exists that mutations introduced are not isolated and could cause unforeseen conformational changes that are responsible for the variants behavior. Crystallization of rfD gives us a structural model of recombinant fibrinogen. It also opens the door to use X-ray crystallography as a tool to examine structural changes in variant fibrinogens of interest because many mutations we have made are located in the D module of the fibrinogen molecule. Structural studies will allow for an understanding of the mutation's impact on protein structure and function. We have crystallized our first mutant fibrinogen, and we are in the process of solving its structure at 2.7 Å.

In conclusion, we have a structural model for fragment D of recombinant fibrinogen and have shown it to be identical to the plasma protein with minor exception. We have also determined the structure of rfD with GPRPam and GHRPam bound and have shown it to be isomorphous with the double-D fragment structure with ligands bound, except for the loss of an important calcium binding site. This study opens the possibility for incisive structure−function studies of engineered mutant fibrinogens.

ACKNOWLEDGMENT

We thank Dr. Matthew R. Redinbo (UNC-CH, Chapel Hill, NC) for critical comments on the manuscript and guidance throughout the project, Dr. David Klapper (UNC-CH) for assistance in determining the sequence of our protein fragment, Dr. Karim C. Lounes for critical comments on the manuscript, Li Fang Ping for her technical assistance, and the National Cell Culture Center for synthesizing the protein.

REFERENCES

1. Doolittle, R. F. (1984) *Annu. Rev. Biochem. 53*, 195−229.
2. Brown, J. H., Volkmann, N., Jun, G., Henschen-Edman, A. H., and Cohen, C. (2000) *Proc. Natl. Acad. Sci. U.S.A. 97*, 85−90.
3. Weisel, J. W., Stauffacher, C. V., Bullitt, E., and Cohen, C. (1985) *Science 230*, 1388−91.
4. Yang, Z., Kollman, J. M., Pandi, L., and Doolittle, R. F. (2001) *Biochemistry 40*, 12515−23.
5. Williams, R. C. (1981) *J. Mol. Biol. 150*, 399−408.
6. Olexa, S. A., and Budzynski, A. Z. (1980) *Proc. Natl. Acad. Sci. U.S.A. 77*, 1374−8.
7. Laudano, A. P., and Doolittle, R. F. (1978) *Proc. Natl. Acad. Sci. U.S.A. 75*, 3085−9.
8. Laudano, A. P., and Doolittle, R. F. (1980) *Biochemistry 19*, 1013−9.
9. Yamazumi, K., and Doolittle, R. F. (1992) *Proc. Natl. Acad. Sci. U.S.A. 89*, 2893−6.
10. Chen, R., and Doolittle, R. F. (1971) *Biochemistry 10*, 4487−91.
11. Budzynski, A. Z., Olexa, S. A., and Brizuela, B. S. (1979) *Biochim. Biophys. Acta 584*, 284−7.
12. Budzynski, A. Z. (1986) *Crit. Rev. Oncol. Hematol. 6*, 97−146.
13. Yee, V. C., Pratt, K. P., Cote, H. C., Trong, I. L., Chung, D. W., Davie, E. W., Stenkamp, R. E., and Teller, D. C. (1997) *Structure 5*, 125−38.
14. Pratt, K. P., Cote, H. C. F., Chung, D. W., Stenkamp, R. E., and Davie, E. W. (1997) *Proc. Natl. Acad. Sci. U.S.A. 94*, 7176−7181.
15. Spraggon, G., Everse, S. J., and Doolittle, R. F. (1997) *Nature 389*, 455−462.
16. Everse, S. J., Spraggon, G., Veerapandian, L., Riley, M., and Doolittle, R. F. (1998) *Biochemistry 37*, 8637−8642.
17. Everse, S. J., Spraggon, G., Veerapandian, L., and Doolittle, R. F. (1999) *Biochemistry 38*, 2941−6.
18. Mosesson, M. W., Hainfeld, J., Wall, J., and Haschemeyer, R. H. (1981) *J. Mol. Biol. 153*, 695−718.
19. Erickson, H. P., and Fowler, W. E. (1983) *Ann. N.Y. Acad. Sci. 408*, 146−63.
20. Veklich, Y. I., Gorkun, O. V., Medved, L. V., Nieuwenhuizen, W., and Weisel, J. W. (1993) *J. Biol. Chem. 268*, 13577−85.
21. Binnie, C. G., Hettasch, J. M., Strickland, E., and Lord, S. T. (1993) *Biochemistry 32*, 107−13.
22. Lord, S. T., Strickland, E., and Jayjock, E. (1996) *Biochemistry 35*, 2342−8.
23. Rooney, M. M., Parise, L. V., and Lord, S. T. (1996) *J. Biol. Chem. 271*, 8553−5.
24. Farrell, D. H., and Thiagarajan, P. (1994) *J. Biol. Chem. 269*, 226−31.
25. Okumura, N., Furihata, K., Terasawa, F., Nakagoshi, R., Ueno, I., and Katsuyama, T. (1996) *Thrombosis Haemostasis 75*, 887−91.
26. Henschen, A. H. (1993) *Thrombosis Haemostasis 70*, 42−7.
27. Gorkun, O. V., Veklich, Y. I., Weisel, J. W., and Lord, S. T. (1997) *Blood 89*, 4407−14.
28. Okumura, N., Gorkun, O. V., and Lord, S. T. (1997) *J. Biol. Chem. 272*, 29596−29601.
29. Laemmli, U. K. (1970) *Nature 227*, 680−5.
30. Everse, S. J., Pelletier, H., and Doolittle, R. F. (1995) *Protein Sci. 4*, 1013−6.
31. Otwinowski, Z. Minor, W. (1997) *Methods Enzymol. 276*, 307−326.
32. Navaza, J. Saludjian, P. (1997) *Methods Enzymol. 276*, 581−594.
33. Brunger, A. T., Adams, P. D., Clore, G. M., DeLano, W. L., Gros, P., Grosse-Kunstleve, R. W., Jiang, J. S., Kuszewski, J., Nilges, M., Pannu, N. S., Read, R. J., Rice, L. M., Simonson, T., and Warren, G. L. (1998) *Acta Crystallogr., Sect. D 54*, 905−21.
34. Brunger, A. T. (1993) *Acta Crystallogr., Sect. D 49*, 24−36.
35. Jones, T. A., Zou, J. Y., Cowan, S. W., and Kjeldgaard, M. (1991) *Acta Crystallogr., Sect. A 47*, 110−119.
36. Read, R. J. (1986) *Acta Crystallogr., Sect. A 42*, 140−149.
37. Townsend, R. R., Hilliker, E., Li, Y. T., Laine, R. A., Bell, W. R., and Lee, Y. C. (1982) *J. Biol. Chem. 257*, 9704−10.
38. Bohme, C., Nimtz, M., Grabenhorst, E., Conradt, H. S., Strathmann, A., and Ragg, H. (2002) *Eur. J. Biochem. 269*, 977−88.
39. Grabenhorst, E., Schlenke, P., Pohl, S., Nimtz, M., and Conradt, H. S. (1999) *Glycoconjugates J 16*, 81−97.
40. Yang, Z., Mochalkin, I., and Doolittle, R. F. (2000) *Proc. Natl. Acad. Sci. U.S.A. 97*, 14156−14161.
41. Hantgan, R. R., and Hermans, J. (1979) *J. Biol. Chem. 254*, 11272−81.
42. Mihalyi, E., and Donovan, J. W. (1985) *Biochemistry 24*, 3443−8.
43. Yakovlev, S., Makogonenko, E., Kurochkina, N., Nieuwenhuizen, W., Ingham, K., and Medved, L. (2000) *Biochemistry 39*, 15730−15741.
44. Madrazo, J., Brown, J. H., Litvinovich, S., Dominguez, R., Yakovlev, S., Medved, L., and Cohen, C. (2001) *Proc. Natl. Acad. Sci. U.S.A. 98*, 11967−72.
45. Mullin, J. L., Gorkun, O. V., Binnie, C. G., and Lord, S. T. (2000) *J. Biol. Chem. 275*, 25239−46.
46. Hogan, K. A., Gorkun, O. V., Lounes, K. C., Coates, A. I., Weisel, J. W., Hantgan, R. R., and Lord, S. T. (2000) *J. Biol. Chem. 275*, 17778−17785.
47. Lounes, K. C., Ping, L., Gorkun, O. V., and Lord, S. T. (2002) *Biochemistry 41*, 5291−9.

BI0261894